RESEARCH ARTICLE

Joint application of seismic refraction and vertical electrical sounding for the delineation of shallow aquifers

Sankar Kumar Nath* and Shamsuddin Shahid

Department of Geology and Geophysics, Indian Institute of Technology, Kharagpur 721 302, India

Inversion of seismic refraction and vertical electrical sounding data alone may lead to incorrect parameter estimation in complex geological set-up, namely, blind zone in seismics, suppression and equivalence in geoelectrics. A unique solution may be achieved by integrating physically different sets of data into a joint or sequential inversion scheme. In this paper we have introduced one such algorithm, wherein the seismic velocity–depth section from ray inversion guides the evolution of a well-resolved geoelectric section in 2D environment from 1D DC resistivity inversion by evolutionary programming. The synthetic models suffering from the suppression and equivalence problems could be successfully reconstructed using this approach. Three test sites at Keshpal, Tata Metalik and Salboni in Midnapur District, West Bengal were selected through remote sensing and GIS tools. By sequentially interpreting the seismic and resistivity data, we could delineate a shallow aquifer with an average thickness of 6.8 m at Tata Metalik. At Salboni, however, a thin aquifer at 46 m depth needed an additional electrolog/litholog depth control for its delineation by the proposed joint approach.

SEISMIC refraction and geoelectric sounding methods can play major roles in evaluation of groundwater resource potential. Although, vertical electrical sounding (VES) is appropriate when geological and hydrogeological units are gently dipping with large lateral extent of minor variation in lithology[1], it fails to solve the equivalence and suppression problems. Seismic refraction prospecting also has its limitations, namely, the failure to identify thin layers (blind zone) and velocity inversion. The limitations in individual techniques can be reduced to a great extent by adopting either joint inversion or multi-sequential inversion schemes. Vozoff and Jupp[2] introduced one such method by combining DC resistivity and magnetotelluric data and observed improved resolution in the estimated model parameters. Different physical quantities can be integrated into a joint or sequential inversion if, at least, the measured data are influenced by a subset of common underground parameters. For example, when using seismic and geoelectrical data representing physically different responses of near-surface features, the layer thickness is the only parameter common to both. The boundary between two layers of different resistivities and seismic velocities may not coincide. Thus, it may occur that, the number of layers derived by independent inversion of seismic and geoelectric data are not identical. However, in order to be sure that geoelectric and seismic data can be combined in a joint inversion scheme, layer-interfaces are assumed[3] to be the same for both geoelectric and seismic properties. Sequential seismic and geoelectric surveys in a coal mine enabled Breitzke *et al.*[4] to correlate the geoelectrical and seismic interfaces within an accuracy of 0.5 m and estimate an improved seismic model using a geoelectrically derived model. Even a coal seam with 24 times higher resistivity than that of the surrounding strata could be unambiguously recognized.

In a joint inversion, different measurement sets are combined to one set before initiating the process of inversion as recorded by Hering *et al.*[3] and Misiek *et al.*[5] for geoelectric and surface wave seismic data. In the multi-sequential inversion, also termed as joint application, we can use the results of one inversion to guide the input to the other. Requirements of a joint inversion are stricter than that of multi-sequential inversion. In the former, both methods must be estimating the same structure, while in the latter some degrees of overlap are required[6]. There are several reports on both the joint inversion[2,3,5,7,8] as well as multi-sequential inversion[1,4,6,9].

A joint application algorithm, multi-sequential in approach, is proposed here to invert seismic refraction travel time data for the delineation of subsurface velocity and interface depths in the first instant. The depth values are passed on to the direct dissemination of VES curves using Koefoed's algorithm[10] to generate a starting model for the subsequent resistivity inversion by Evolutionary Programming (EP). Beard and Morgan[11] indicated that 2D subsurface geometry can be approximately delineated using contours based on apparent resistivity and 1D inversion. In the present investigation,

*For correspondence. (e-mail: nath@gg.iitkgp.ernet.in)

seismic ray inversion provides 2D control over the 1D inversion of VES data. For the construction of final subsurface model seismic layer thicknesses and sequentially inverted resistivity values are considered as parameters. One major aim of this investigation being the delineation of aquifers, two synthetic models as well as real field examples from Keshpal and Tata Metalik areas in Midnapur District, West Bengal were chosen for groundwater resource studies.

The test sites were selected on the basis of hydrogeological inputs, e.g. litholog, drainage density, slope, soil composition, their proximity to river Kasai and the geological depositional sequence favourable for shallow groundwater potential zone. To validate this integration approach for deeper aquifers facing constraints of blind zone in seismic and equivalence/suppression in electrical method, another test site is selected at Salboni where electrical log or litholog data are used for depth control. However, the present software is applicable to any geological set-up without depth restriction. The limitation is posed mainly by the seismic data due to the limited penetration power of the mechanical seismic sources used for refraction analysis.

Theory and algorithm

Ray inversion for near surface estimation (RINSE) from seismic refraction data

RINSE[12] uses headwave travel times from multi-fold seismic refraction data and the average velocity in the layer above the refractor to determine the shape of the boundary. The slopes of headwave travel time curves are used to estimate the direction of refracted waves arriving at the surface and leaving the source. Travel times computed along pairs of intersecting rays from the source to receivers, near the source, are compared with observed travel times to reconstruct the shape of the first refractor boundary beneath the surface and the variation in seismic velocity along this boundary. This theoretical information is used as a basis for further processing to calculate depth and velocity variations along the remaining refractors by downward continuation of the refracted rays[13]. The present algorithm is coded in *Visual C++* with a provision to determine the number of layers from channel to channel critical distance (X_c) variation. For X_c computation RINSE uses backward continuation to project headwave arrival times to near offsets where they are not recorded as first arrivals. The X_c value remains constant for all the refracted arrivals from the same interface, but is marked by an abrupt change when the arrivals come from a different interface. Plotting of X_c values helps the interpreter select channel numbers at which the arrivals come from different layers and in a way, to assess the total number of layers also. Once the depth points of the first interface are determined, the observation plane is lowered and the travel time curves are reduced to conform to the new observation plane. The depth points are calculated and the observation plane is lowered further till the travel time data are completely exhausted. Thus, all the subsurface lithounits are delineated with their velocities derived from the slopes.

Dissemination of VES curve using Koefoed's algorithm by seismic depth control

Using seismic layer thickness a VES curve can be disseminated by Koefoed's algorithm[10] as follows:

(1) Computation of sample values of resistivity transform from the observed apparent resistivity data using a linear filter.
(2) Calculation of the top layer resistivity from the early part of the resistivity transform curve using the following expression:

$$\rho_i = \frac{1}{2}A(T_i - T_i') + \sqrt{\frac{1}{4}A^2(T_i - T_i')^2 + T_i T_i'}; \quad (1)$$

where T_i is resistivity transform of the first sampling point, T'_i is resistivity transform of the next sampling point, and $A = \text{cotanh}[(\lambda - \lambda')h]$, such that, λ is abscissa of the first sampling point, λ' is abscissa of the next sampling point, and h is seismic layer thickness.

(3) Reduction of the resistivity transform curve to a lower boundary plane.
Steps (2) and (3) are iterated until the transform curve has been exhausted.

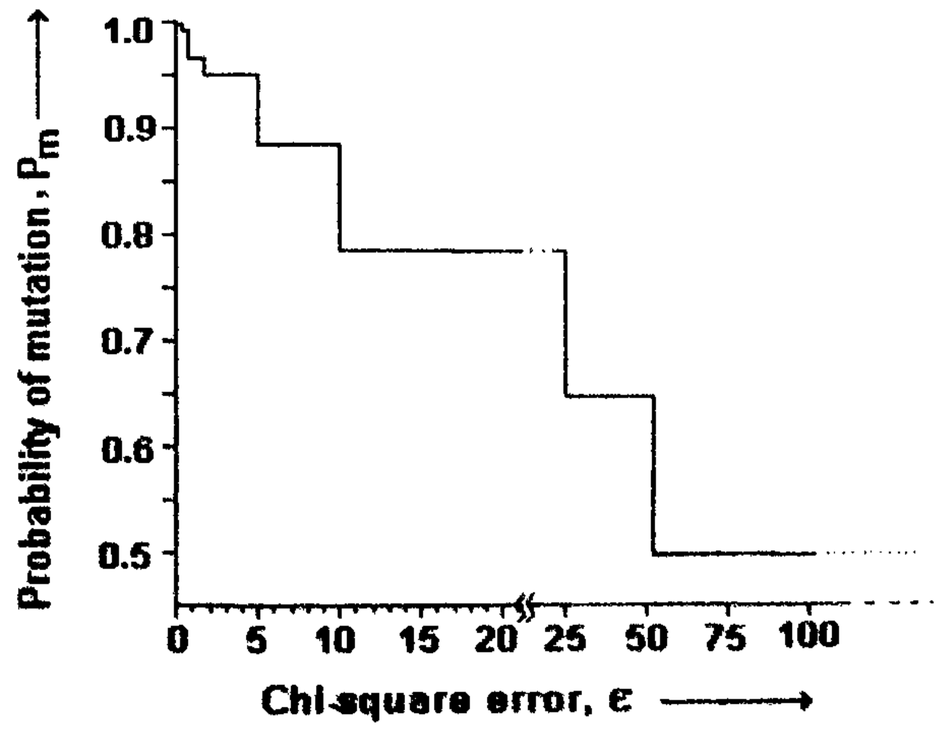

Figure 1. Step function for probability of mutation.

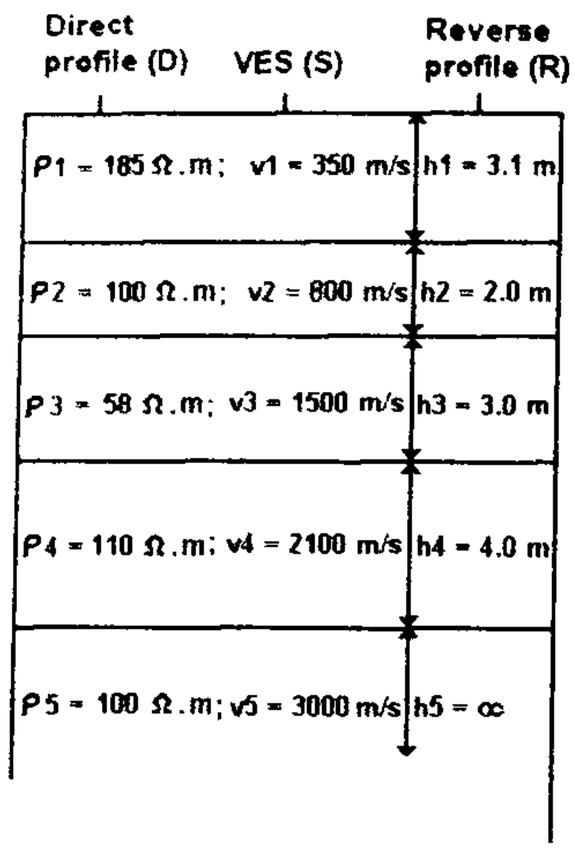

a

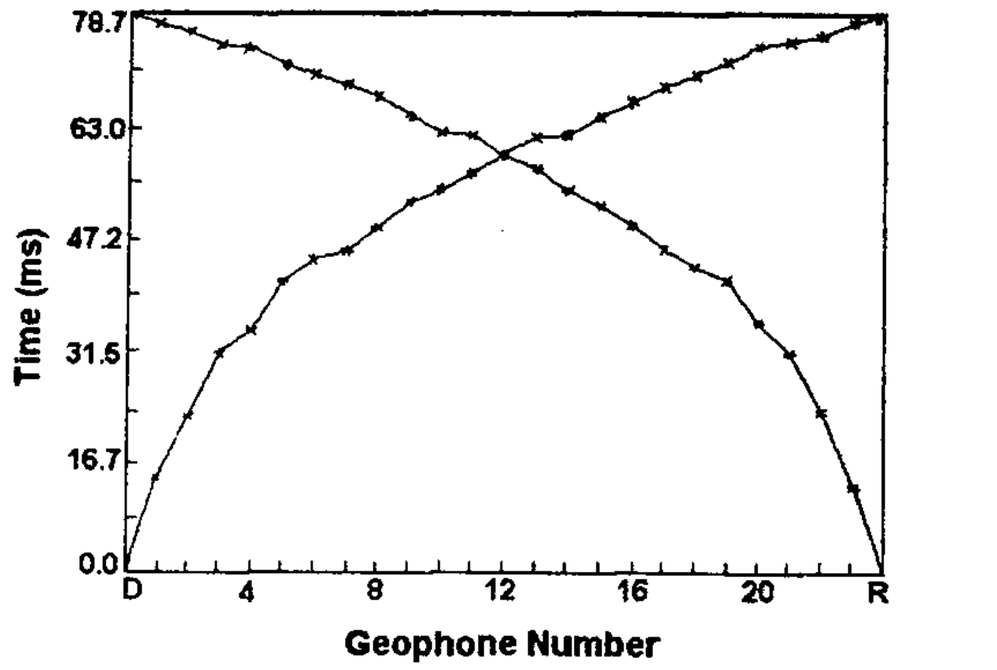

b

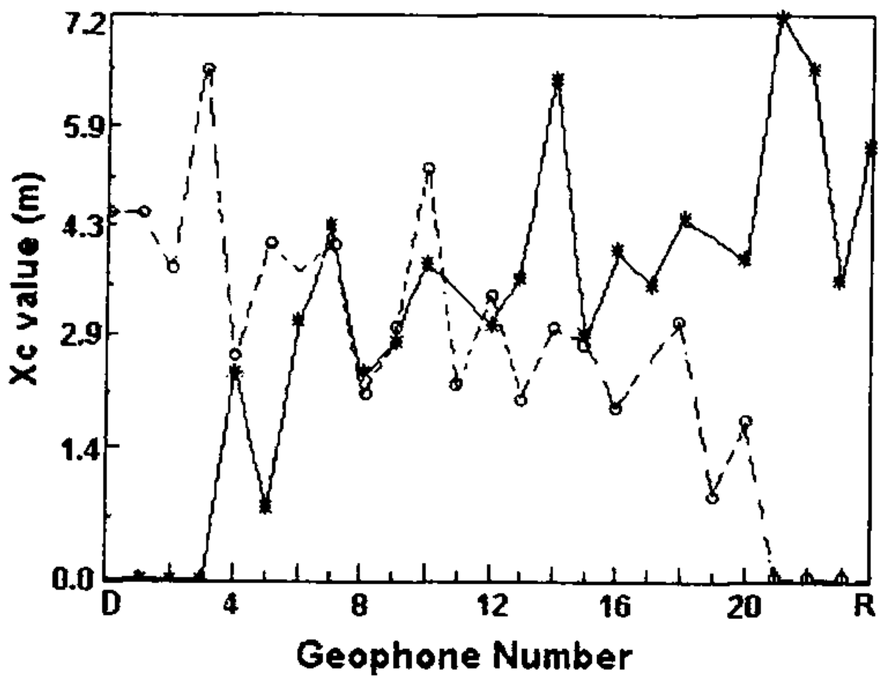

c

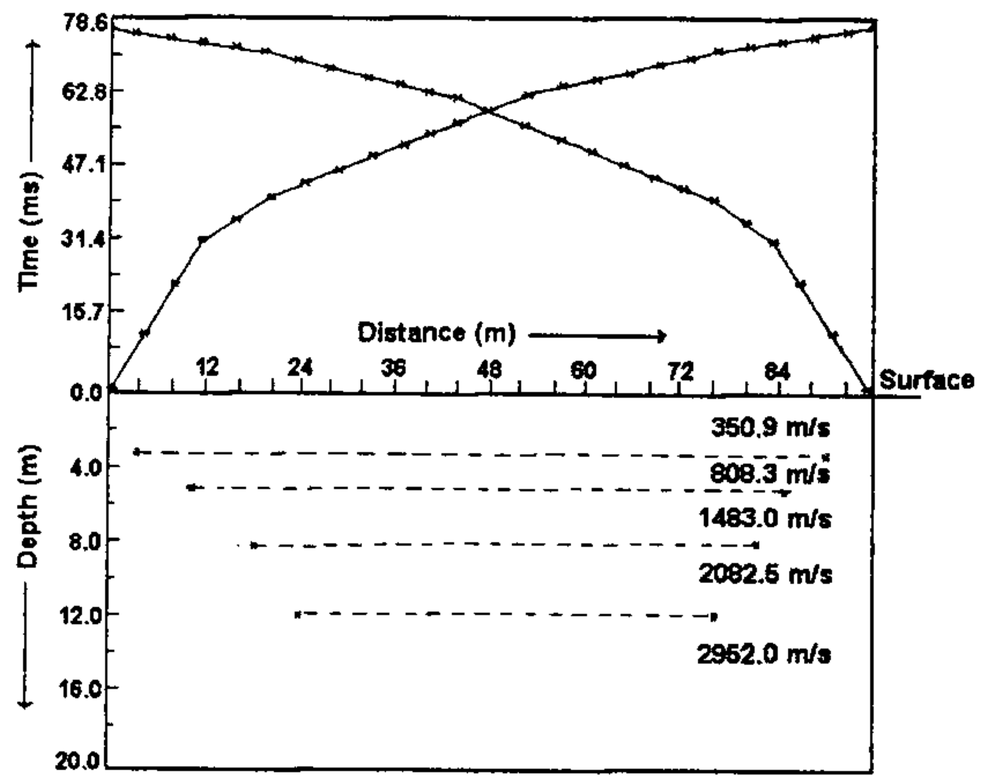

d

e

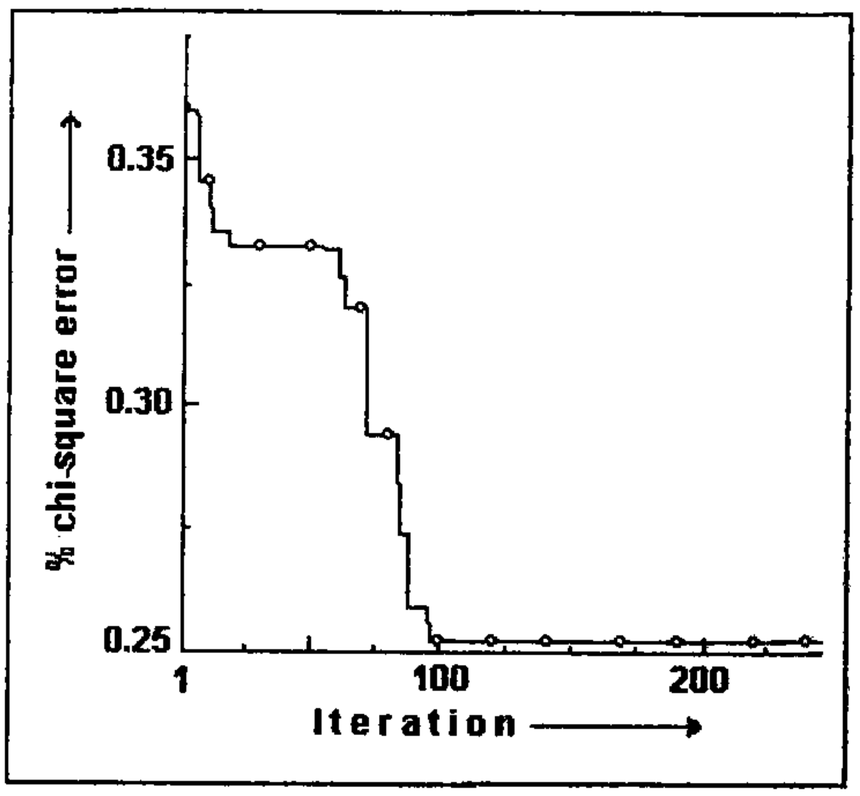

f

Figure 2 *a*, Five-layer earth model configuration and physical parameters; *b*, Time–distance curves for direct and reverse shot pair with a ± 10% Gaussian noise added; *c*, X_c plot of noisy travel time data for direct and reverse shot pair; *d*, Smoothened time–distance curves and interpreted velocity–depth section for the model; *e*, Theoretical and estimated VES curves by sequential and curve matching techniques for the model; *f*, Variation of % chi-square error with iteration during evolutionary process.

Interpretation of VES data using EP

Genetic Algorithm (GA)[14,15] belongs to the group of random search techniques such as Monte Carlo, Simulated Evolution, Simulated Annealing and Very Fast Simulated Annealing[16] guided by the stochastic process to help the system learn the minimum path and explore the model space extensively. But the difficulty with GA lies in the premature convergence which can be solved by EP[17].

In DC resistivity sounding we are concerned with the parameters $\rho_1, \rho_2, \ldots, \rho_n$ and $h_1, h_2, \ldots, h_{n-1}$. EP[18] evolves the exact solution of each parameter within a pair of bounds using the following three steps.

Generation of population: The n real coded individuals in the population are generated randomly within the user defined parameter bounds, population size and randomization seed number.

Computation of fitness: Fitness function of each individual of the population is estimated from the chi-square error ε defined as,

$$\varepsilon = \frac{1}{N}\left(\frac{\rho_a^{com} - \rho_a^{obs}}{\rho_a^{com}}\right)^2 \qquad (2)$$

where, $\rho_a{}^{com}$ is calculated apparent resistivity values by Ghosh's linear filter[19], $\rho_a{}^{obs}$ is observed apparent resistivity data, and N is number of observations.

Mutation: An equal number of individuals are generated by perturbing each member of the population by step function mutation. The mutation value is assigned depending on the fitness ($1/\varepsilon$) of the individual. After several tests, the probability of mutation P_m is found to yield better convergence if a step like distribution is used as shown in Figure 1.

After each iteration n newly generated models are mixed with those from the previous iteration to form $2n$ models. The best n models are retained for the next iteration. The second and third steps mentioned earlier are repeated until a threshold error or iteration limit is reached.

Joint application

The algorithms of seismic ray inversion[13], dissemination of VES curves by Koefoed's technique[10] and resistivity inversion by EP[18] are combined together as a joint application routine, multi-sequential in nature, for the systematic evaluation of aquifers. The software follows three major steps.

(1) Subsurface parameterization in terms of depth and velocity distribution through RINSE.

(2) Initial geoelectric model generation from layer resistivity values through curve dissemination and layer thickness values from step (1).

(3) Addition of a $\pm 20\%$ perturbation to the initial seismo-electric section from step (2) for defining the pair of bounds of the solution. This is important as EP evolves the final solution out of a randomly generated population within this preset range. This takes care of any appreciable differences arising between the seismic and geoelectric boundaries. In case the initial guess values are derived from noisy data, the prescribed perturbation enhances the possibility of getting closer to the correct solution.

A seismo-electric panel diagram is the final output of this program.

Results and discussion

Synthetic examples

It is routine to use synthetic examples for testing the performance of any inversion algorithm. The present joint application program is rigorously tested on a variety of numerical models, of which two cases are presented here. Synthetic headwave arrival times from source to geophones are computed for an array of 24 channels at 4 m receiver spacing for direct and reverse shot pairs. VES curves are generated using Ghosh's linear filter method.

Model I: Figure 2 *a* presents the configuration and physical parameters of a five-layer earth model. In this model the second layer resistivity is intermediate between that of the first and the third layers, thereby depicting a suppression problem. The resistivity contrast between the fourth and fifth layers is also negligible. The synthetic travel time curves for the direct and reverse shots with a $\pm 10\%$ Gaussian noise added are shown in Figure 2 *b*. The X_c plots for both the shots from RINSE are displayed in Figure 2 *c*. Using these X_c values the time–distance curves are smoothened. A new X_c plot is generated for picking the change over points, which in this case are at channels 3, 5, 13 and 20. Invoking the downward continuation, subsurface points on all the four refractors are traced and joined. The velocity distribution in all the five layers, the estimated depth section together with the smoothened time–distance curves are displayed in Figure 2 *d*. Comparison of the seismic velocity–depth section with the original model shows a more or less complete match. The noisy synthetic VES curve for the model is QHK-type (Figure 2 *e*). Using the depth values from seismic section of Figure 2 *d* the curve is disseminated by Koefoed's modified resistivity transform method. The actual layer

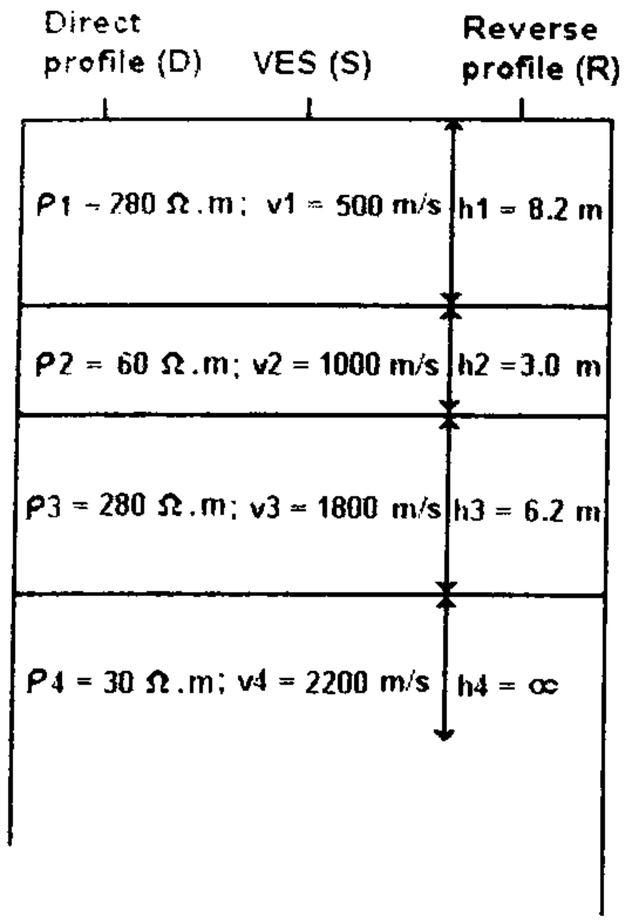

a

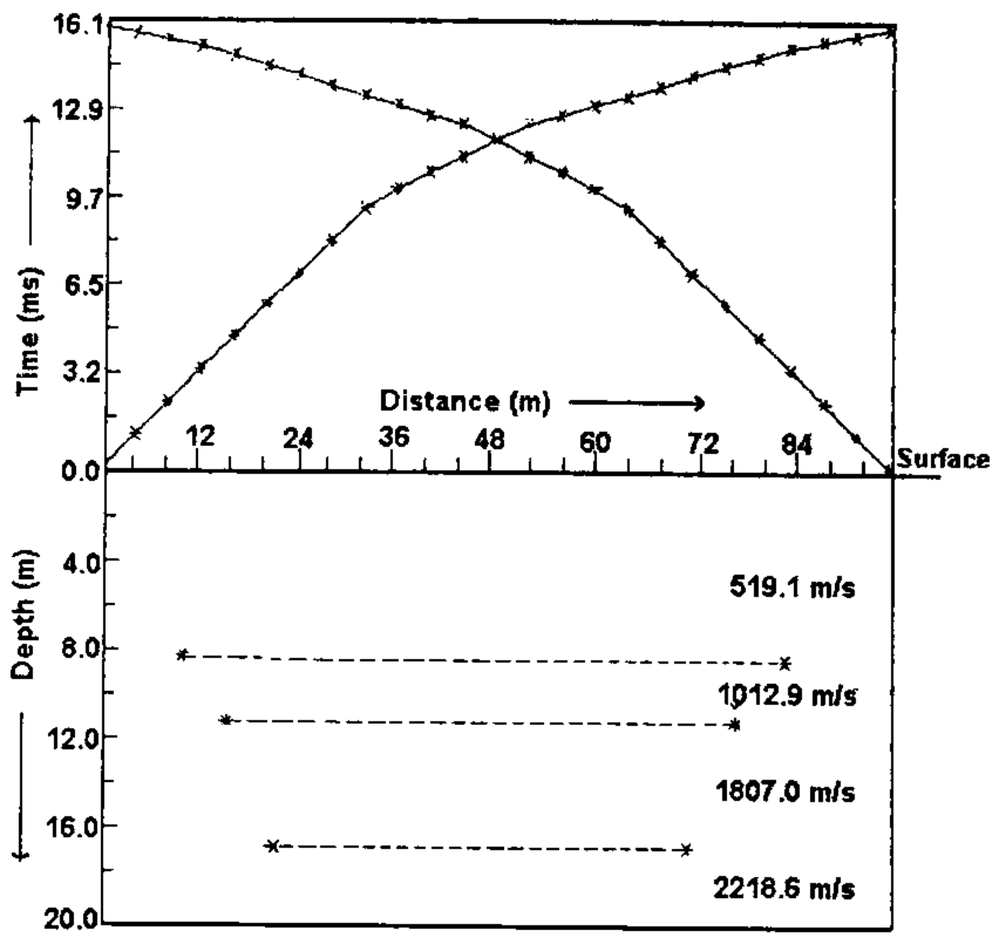

b

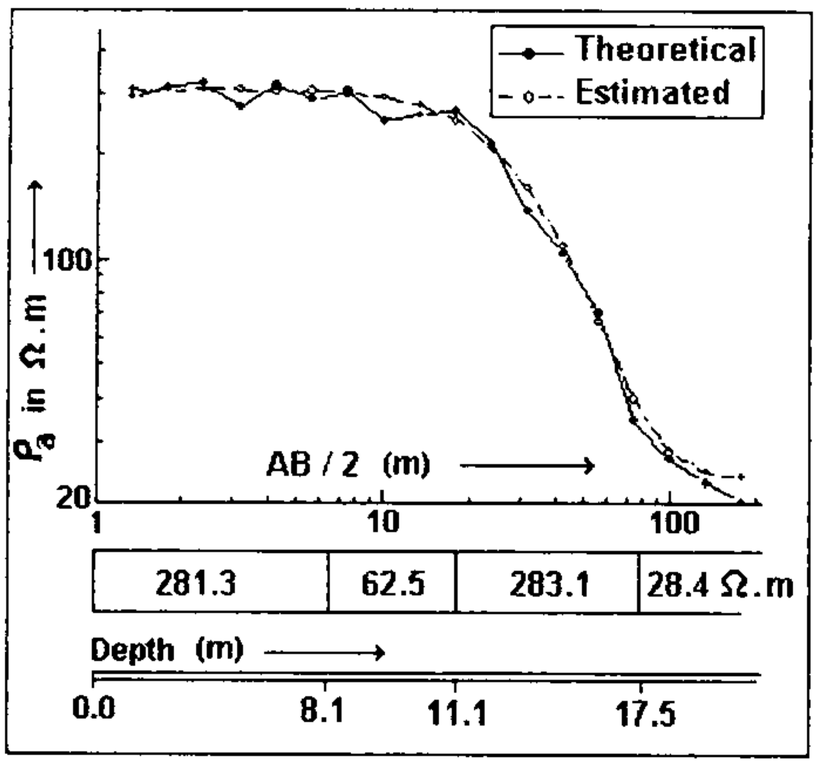

c

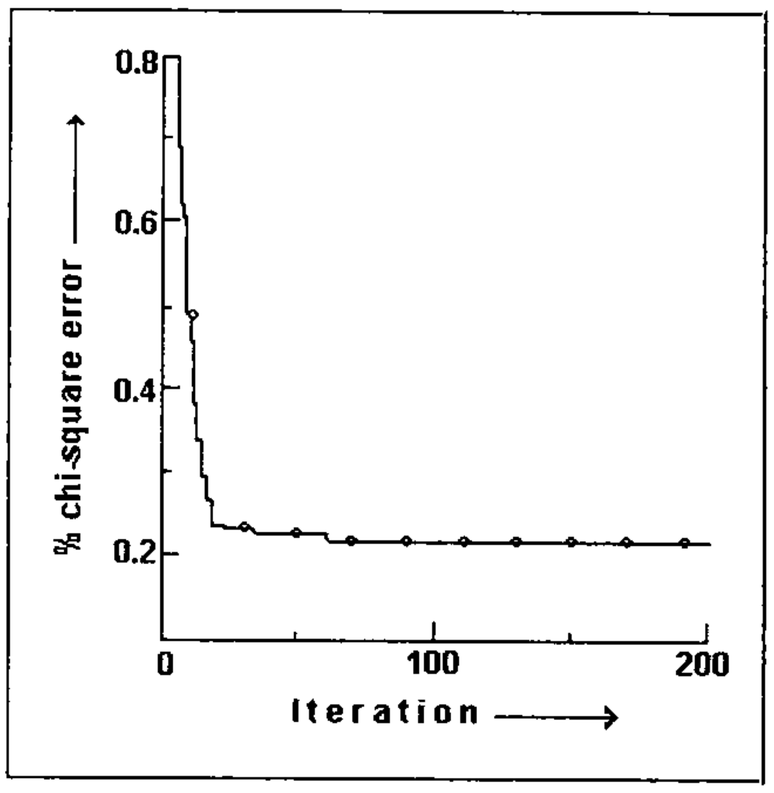

d

Figure 3 *a*, Four-layer earth model configuration and physical parameters; *b*, Time–distance curves and interpreted velocity–depth section for the model; *c*, Theoretical and estimated VES curves for the model; *d*, Variation of % chi-square error with iteration during evolutionary process.

parameters and those obtained by seismic, curve dissemination, EP and conventional curve matching techniques are compared in Table 1 with the corresponding theoretical and estimated VES curves been presented in Figure 2 *e*. The sequential error curve is shown in Figure 2 *f*. It is certain that the curve matching and VES inversion would have generated only a four-layer earth model, which in this case would have been a wrong prediction. Therefore, the joint application routine could solve an intricate geoelectric problem posed by this model.

Model II: The model shown in Figure 3 *a* presents a four-layer geological setting from seismic point of view. There is a conductive bed in a resistive set-up. The bottom layer is also highly conductive. This may be viewed as the inclusion of a sandy lens in the gravelly layer on top of a clay bed. Geoelectrically, this looks like a two-layer earth model. But using the seismic depth section of Figure 3 *b* from RINSE all the four layers could be delineated with their parameters listed in Table 1 and the theoretical and estimated VES curves in Figure 3 *c*. The sequential inversion error curve is displayed in Figure 3 *d*.

Table 1. Seismic and geoelectric parameters of the synthetic models

Model no.	Estimate	v_1 (m/s)	v_2 (m/s)	v_3 (m/s)	v_4 (m/s)	v_5 (m/s)	ρ_1 (Ω.m)	ρ_2 (Ω.m)	ρ_3 (Ω.m)	ρ_4 (Ω.m)	ρ_5 (Ω.m)	h_1 (m)	h_2 (m)	h_3 (m)	h_4 (m)	h_5 (m)
I	Original layer parameters	350	800	1500	2100	3000	185	100	58	110	100	3.1	2.0	3.0	4.0	∞
	Seismic (RINSE)	351	808	1483	2082	2952	–	–	–	–	–	3.1	2.0	3.0	4.0	∞
	Initial model (curve dissemination)	–	–	–	–	–	201	84	47	98	94	3.2	1.9	3.2	3.8	∞
	Geoelectric model (sequential)	–	–	–	–	–	187	97	56	106	98	3.1	2.0	3.1	4.2	∞
	Geoelectric model (curve matching)	–	–	–	–	–	196	45	124	76	–	4.8	3.2	3.9	∞	–
II	Original layer parameters	500	1000	1800	2200	–	280	60	280	30	–	8.2	3.0	6.2	∞	–
	Seismic (RINSE)	519	1013	1807	2219	–	–	–	–	–	–	8.2	2.9	6.0	∞	–
	Initial model (curve dissemination)	–	–	–	–	–	294	70	269	11	–	8.0	2.8	3.4	∞	–
	Geoelectric model (sequential)	–	–	–	–	–	281	62	283	28	–	8.1	3.0	6.4	∞	–

Field examples

The study area in Midnapur District is situated on a mild topographic high and is covered mainly by three types of lithology, viz. laterite, old alluvium and new alluvium. A reconnaissance survey is conducted using remote sensing technique. IRS-IB, LISS-II data are processed and enhanced using ERDAS software. A standard False Colour Composite (FCC) (bands 1, 2 and 3) was prepared for the drainage density map of the area as shown in Figure 4 *a*. A Principal Component Composite (PCC) of bands 1, 2 and 3 is used to identify the geological and geomorphological features of the area and generate the thematic maps (Figure 4 *b*). Geographic Information System (GIS) analysis of these maps predicted the distributed shallow groundwater potential zones in the area. Keshpal and Tata Metalik (Figure 5 *a*) are two such sites with moderate habitation surviving on tapping shallow groundwater. While Keshpal is situated on the young terrace, Tata Metalik is on the old terrace of river Kasai. Both the sites have low drainage density and are covered by loamy soil favourable for shallow groundwater potential. A third site is selected at Salboni (Figure 5 *a*), 7 km north-west of Midnapur town for validating the potential of this algorithm in delineating a thin aquifer at a depth of 46 m as observed on electrical logs and litholog.

Data acquisition

VES data were collected using Schlumberger electrode configuration with a maximum spacing (AB/2) from 150 to 400 m. Using a OYO McSeis-160 signal enhancement 12/24 channel seismograph and a weight dropper source seismic data were acquired in the field. At Keshpal two VES and one seismic profile with 24 channels at 4 m geophone spacing were taken. The profile layout is shown in Figure 5 *b*. At Tata Metalik thirteen VES and two cross seismic profiles with a 12-channel layout at 6 m spacing shown in Figure 5 *c* were conducted. At Salboni, situated on a typical lateritic terrain, one VES and one seismic profile with 24 channel layout (Figure 5 *d*) at 5 m geophone spacing were taken.

Field testing at Keshpal site

In Figure 6 *a* the time–distance curves for three direct and three reverse shots (32 m shot spacing) and the interpreted velocity–depth section by ray inversion technique are presented. The subsurface layer parameters from seismic, sequential inversion and conventional curve matching at S1 and S2 survey locations are listed in Table 2 with the observed and calculated VES curves given in Figure 6 *b* and the error curves in Figure 6 *c*. It is evident from Figure 6 *b* that the sequentially estimated VES curves are closer to the observed ones than those obtained by curve matching.

Delineation of aquifer at Tata Metalik site

Figure 7 *a* presents the time–distance curves for six direct–reverse shot pairs (36 m shot interval) of the seismic profile R1 and the interpreted velocity–depth section. Three sample VES curves at S3, S4 and S5 are shown in Figure 7 *b*. The estimated layer parameters from RINSE and sequential inversion are given in

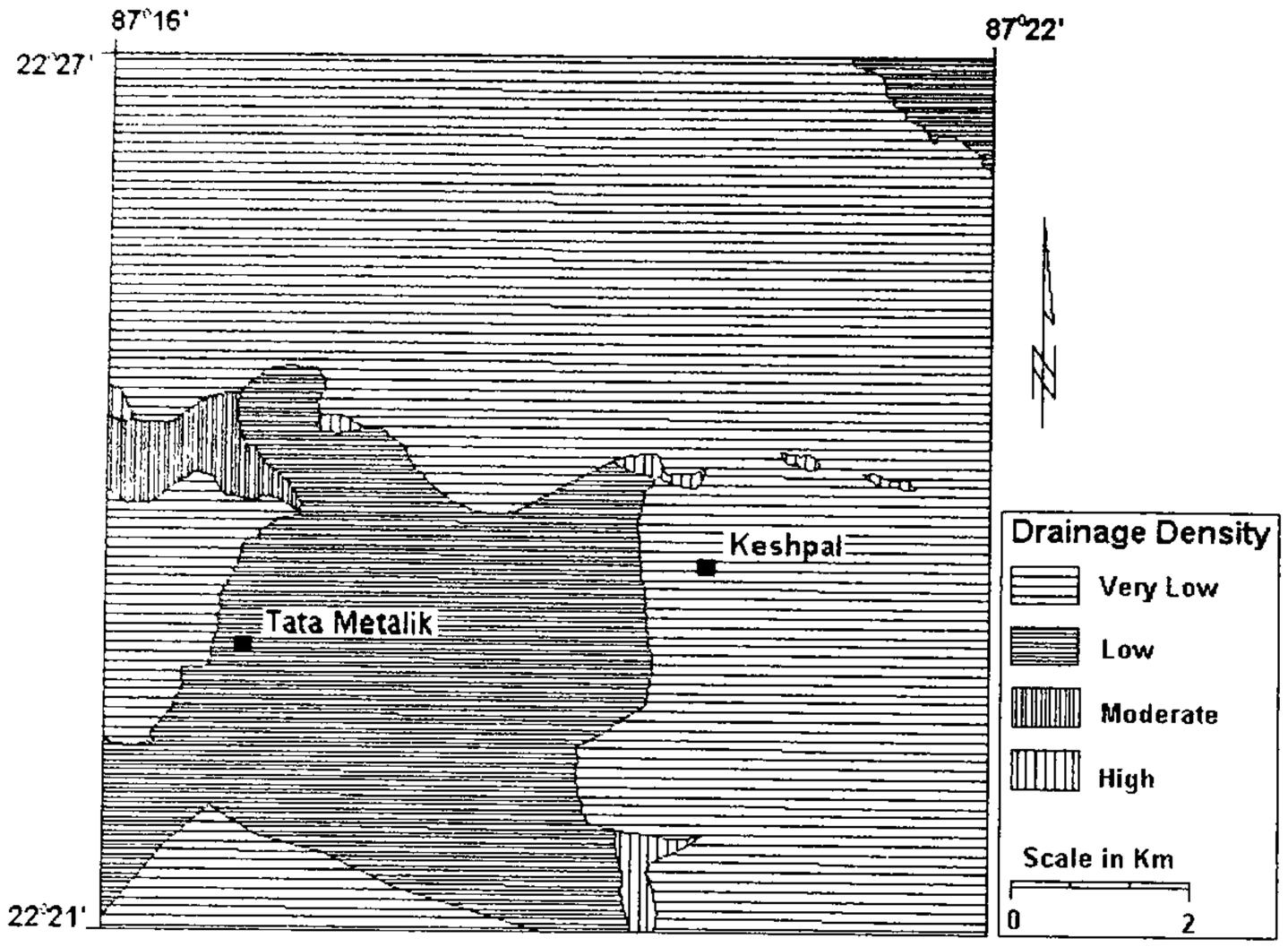

a

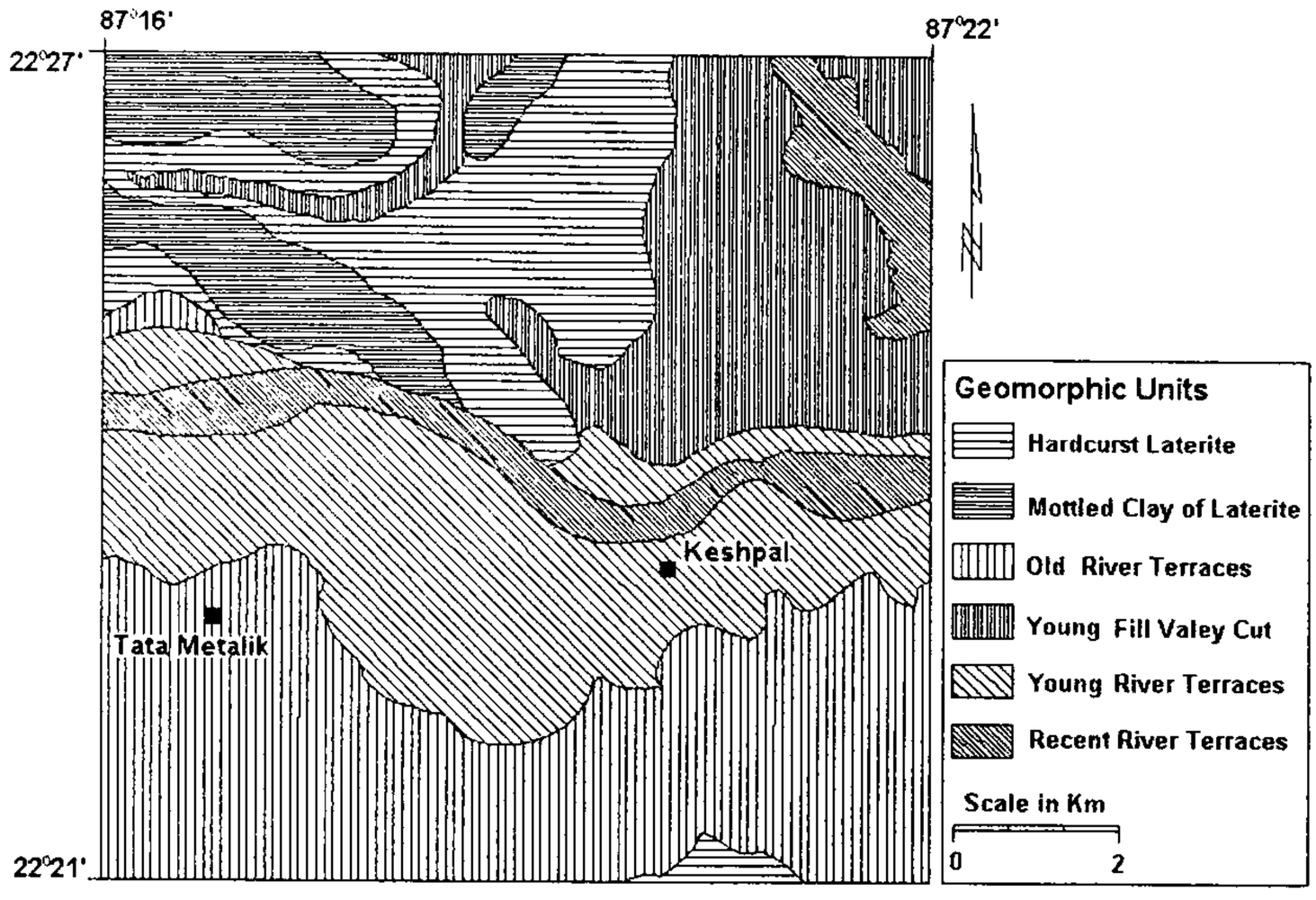

b

Figure 4. Thematic map of *a*, drainage density and *b*, geomorphology of the study area from IRS-1B data.

Table 2. Seismic and geoelectric parameters at Keshpal

	Seismic layer parameters from RINSE						Geoelectric layer parameters from sequential inversion						Geoelectric layer parameters from curve matching					
Position	v_1 (m/s)	v_2 (m/s)	v_3 (m/s)	h_1 (m)	h_2 (m)	h_3 (m)	ρ_1 (Ω.m)	ρ_2 (Ω.m)	ρ_3 (Ω.m)	h_1 (m)	h_2 (m)	h_3 (m)	ρ_1 (Ω.m)	ρ_2 (Ω.m)	ρ_3 (Ω.m)	h_1 (m)	h_2 (m)	h_3 (m)
S1	666	1333	2000	2.7	15.3	∞	23.8	74.5	10.1	2.8	15.2	∞	21.2	90.2	5.6	3.9	17.2	∞
S2	666	1333	2000	4.9	15.0	∞	27.1	126.6	7.9	4.8	15.0	∞	34.5	189.0	6.3	5.4	14.7	∞

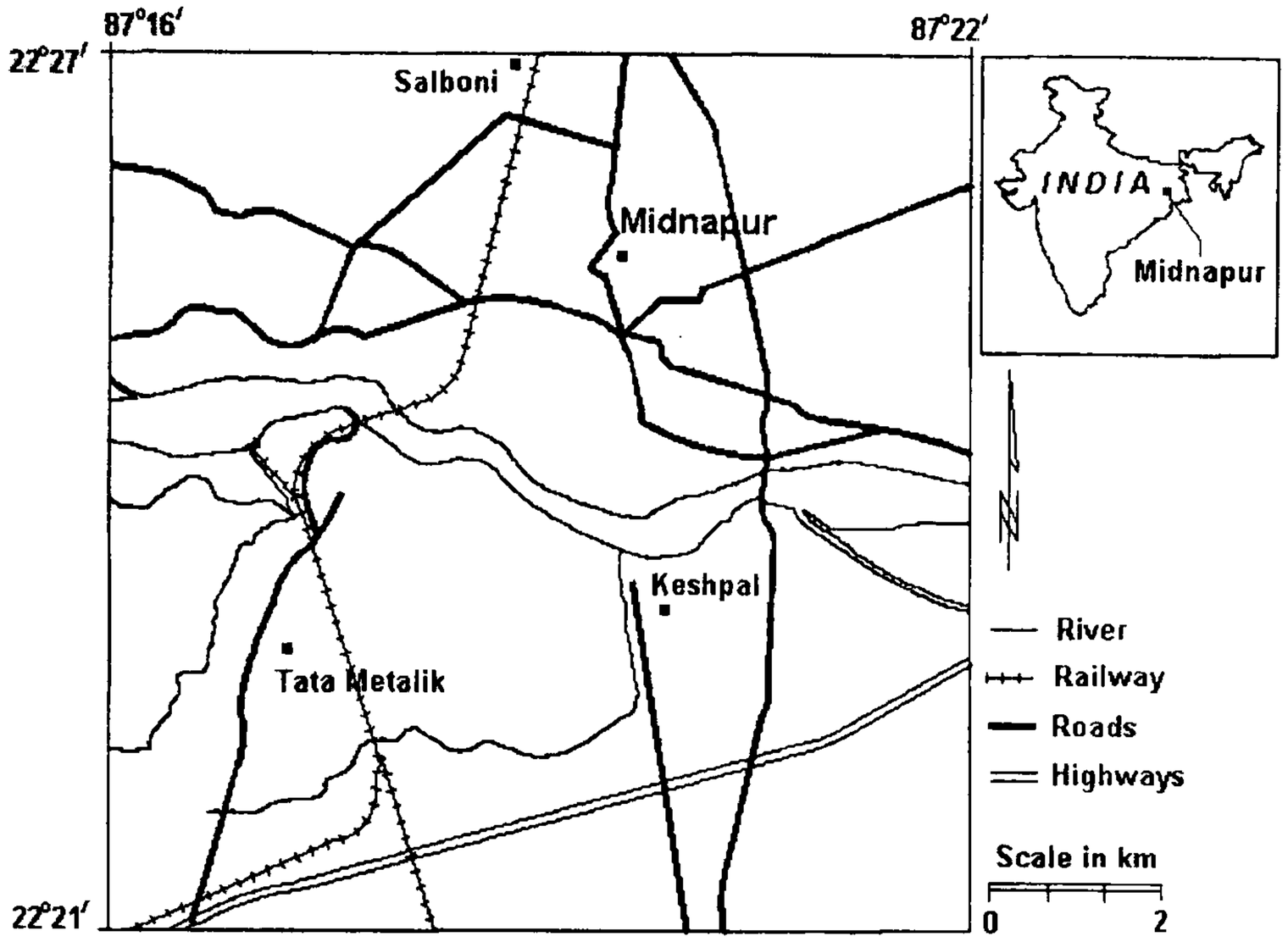

a

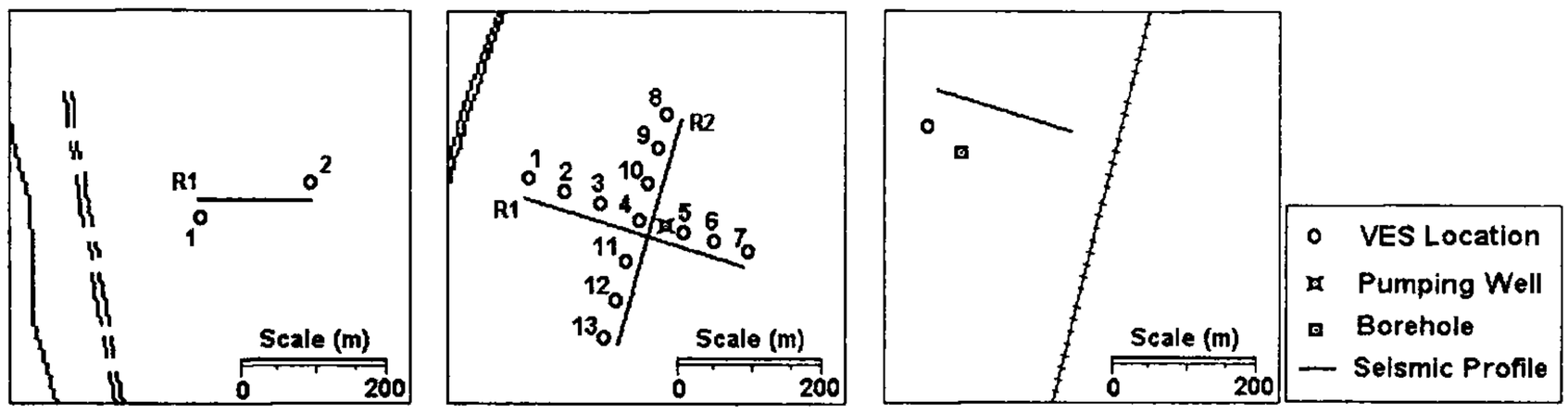

b *c* *d*

Figure 5 *a*, Location map of the study area in Midnapur District, West Bengal. Seismic profiles and VES layout at *b*, Keshpal; *c*, Tata Metalik, and *d*, Salboni.

Table 3. Seismic and geoelectric parameters at Tata Metalik

		Seismic layer parameters from RINSE						Geoelectric layer parameters from sequential inversion					
Seismic profile ID	VES position	v_1 (m/s)	v_2 (m/s)	v_3 (m/s)	h_1 (m)	h_2 (m)	h_3 (m)	ρ_1 (Ω.m)	ρ_2 (Ω.m)	ρ_3 (Ω.m)	h_1 (m)	h_2 (m)	h_3 (m)
R1	S1	345	866	2650	2.1	6.8	∞	10.2	42.5	14.0	2.2	6.9	∞
	S2	345	866	2650	1.7	6.7	∞	9.7	47.4	19.3	1.6	6.8	∞
	S3	345	866	2650	1.1	6.3	∞	8.8	46.4	16.0	1.0	6.1	∞
	S4	345	866	2650	2.5	6.3	∞	12.2	40.1	19.8	2.5	6.4	∞
	S5	345	866	2650	3.4	5.3	∞	10.0	44.1	13.2	3.3	5.2	∞
	S6	345	866	2650	3.8	4.6	∞	13.1	52.0	17.8	3.8	4.7	∞
	S7	345	866	2650	3.5	5.4	∞	11.7	49.0	14.3	3.6	5.3	∞
R2	S8	353	892	2657	2.2	9.8	∞	10.3	43.3	20.0	2.2	9.7	∞
	S9	353	892	2657	2.5	8.8	∞	14.2	54.2	17.5	2.5	8.9	∞
	S10	353	892	2657	1.5	7.8	∞	8.2	40.3	18.2	1.4	7.8	∞
	S11	353	892	2657	3.7	5.5	∞	9.9	41.0	16.0	3.9	5.4	∞
	S12	353	892	2657	3.1	7.4	∞	13.8	45.6	15.2	3.0	7.6	∞
	S13	353	892	2657	3.2	7.8	∞	11.1	42.0	16.4	3.2	7.6	∞

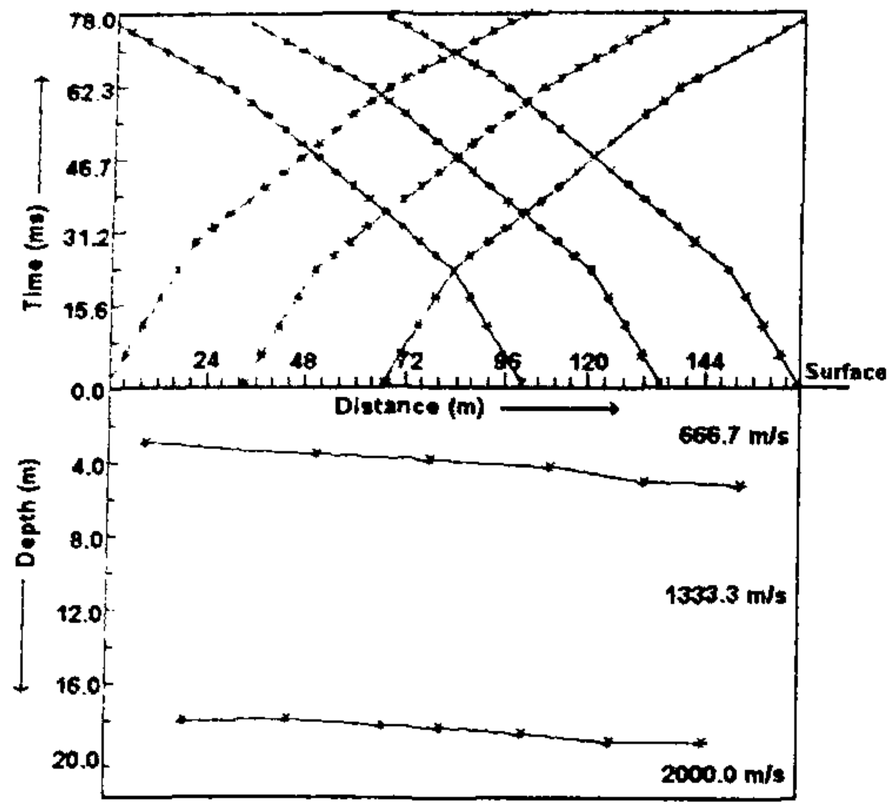

a

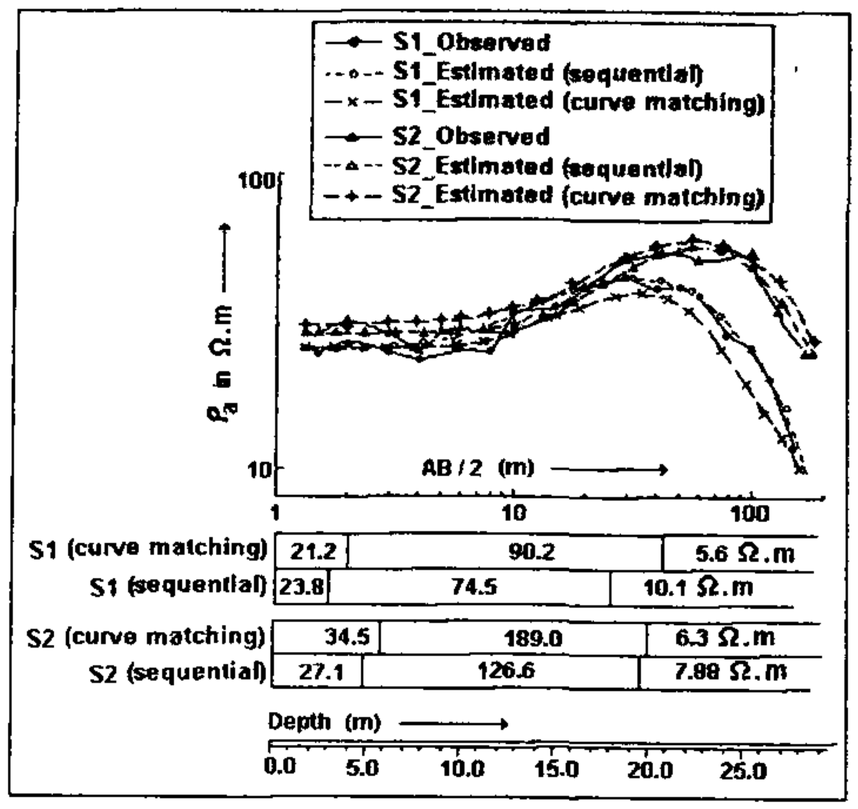

b

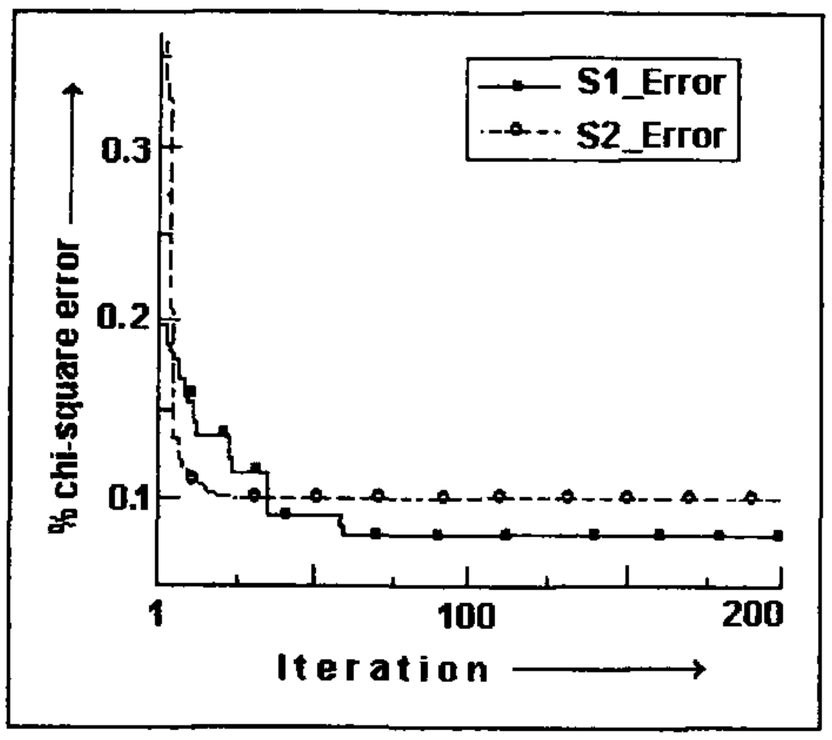

c

Figure 6 *a*, Time–distance curves and interpreted velocity–depth section for profile R1 at Keshpal; *b*, Observed and estimated VES curves by sequential and curve matching techniques at S1 and S2 at Keshpal; *c*, Error curves for VES inversion at S1 and S2.

Table 3 at all the thirteen VES locations. The calculated and observed curves at S3, S4 and S5 are in good agreement as evident from Figure 7 *b* with the error curves in Figure 7 *c*. The seismic depth section and the corresponding resistivity values of thirteen VES curves are integrated in the form of a panel diagram displayed in Figure 8 *a* to develop a 3D model of the seismo-electric setting of Tata Metalik area. The middle sand layer is the probable aquifer with an average thickness of 6.8 m having the P-wave velocity of 867 m/s and a resistivity range of 40–55 Ω m. This finding is later corroborated by the litholog (Figure 8 *b*) of the pumping well.

Delineation of aquifer at Salboni from electrical log/litholog depth control

Salboni was selected as a test site for the present integration approach to delineate deeper aquifers where one may face the constraints of blind zone in seismic and equivalence/suppression in geoelectrical prospecting. One seismic profile and one electrical sounding were conducted in this area. In Figure 9 *a* the time–distance curve for two direct-reverse shot pairs (30 m shot spacing) and a four-layer velocity–depth section from RINSE are presented. Electrical logs, both SP and point resistance and litholog shown in Figure 9 *b* were avail-

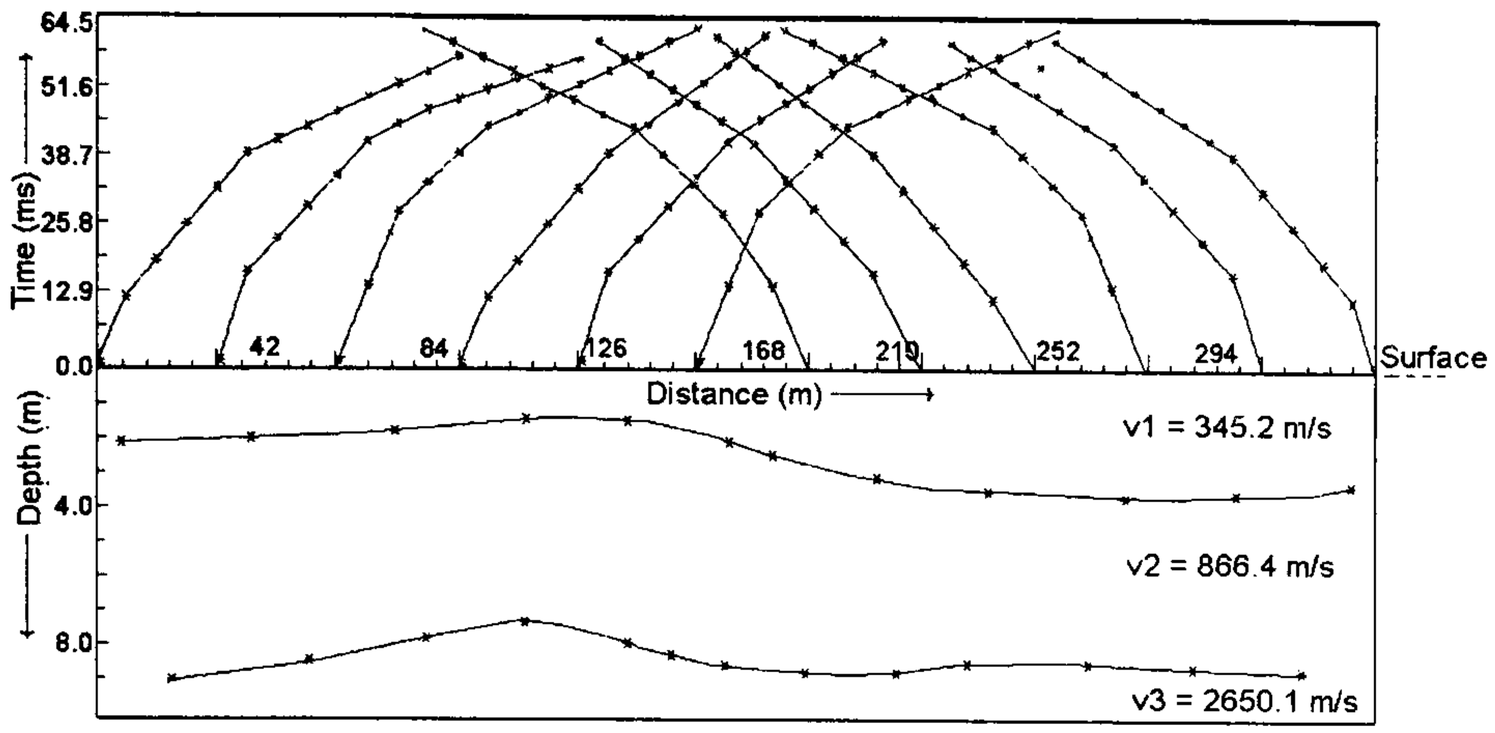

a

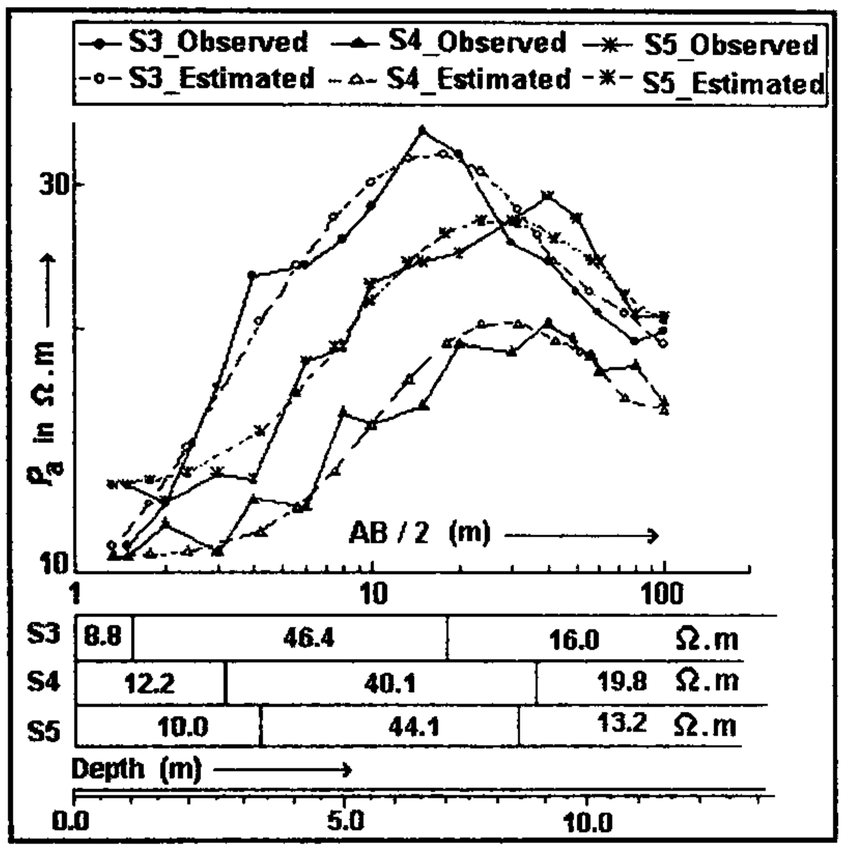

b

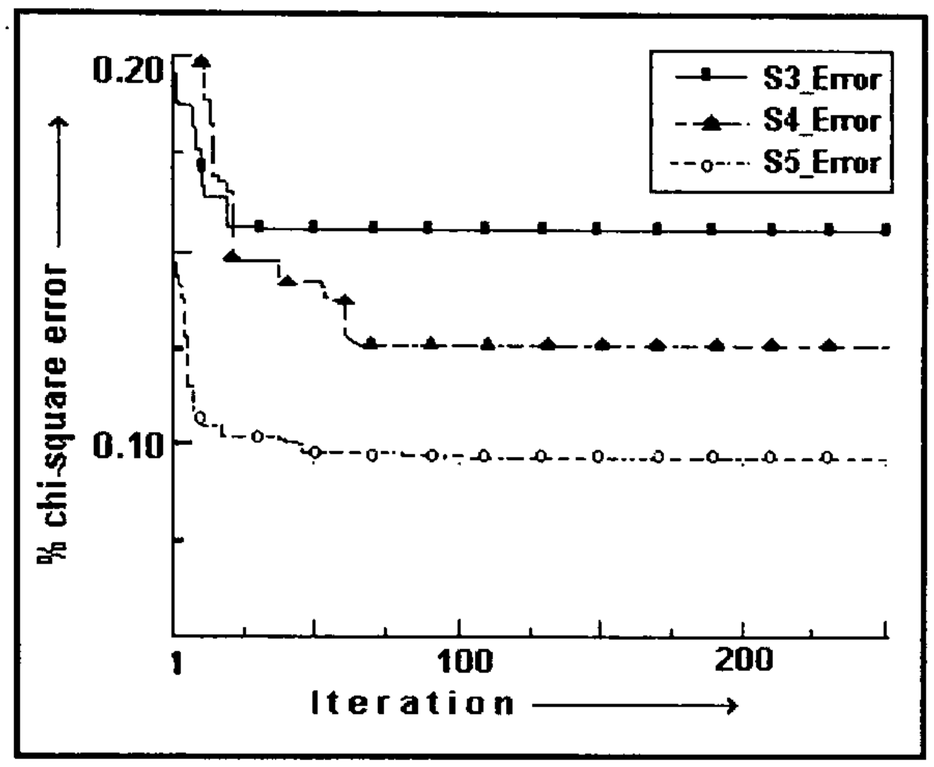

c

Figure 7 *a*, Time–distance curves and interpreted velocity–depth section for profile R1 at Tata Metalik; *b*, Observed and estimated VES curves at S3, S4 and S5 at Tata Metalik. *c*, Error curves for VES inversion at S3, S4 and S5.

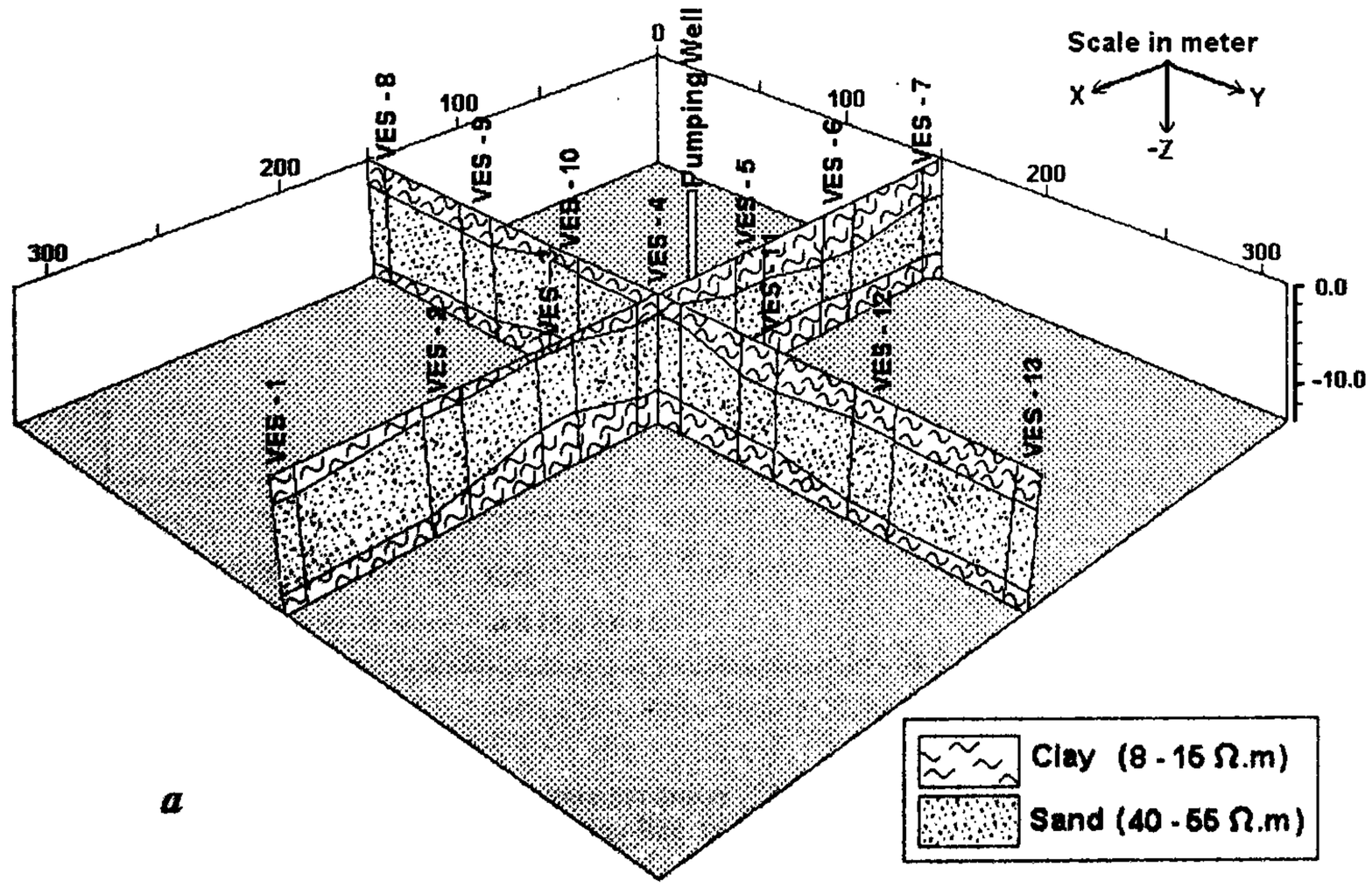

a

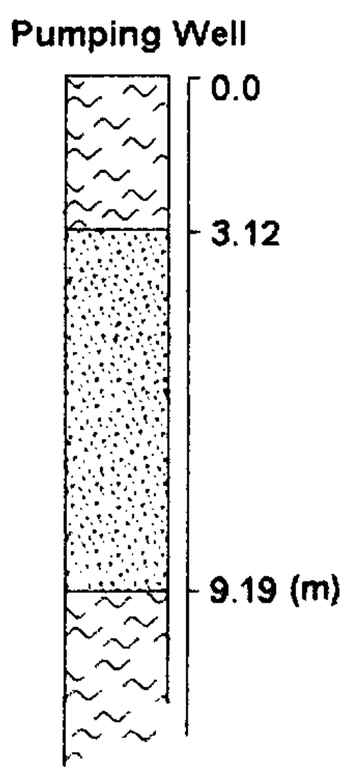

b

Figure 8 *a*, Three-dimensional seismo-electric model of Tata Metalik area; *b*, Pumping well litholog at the same site.

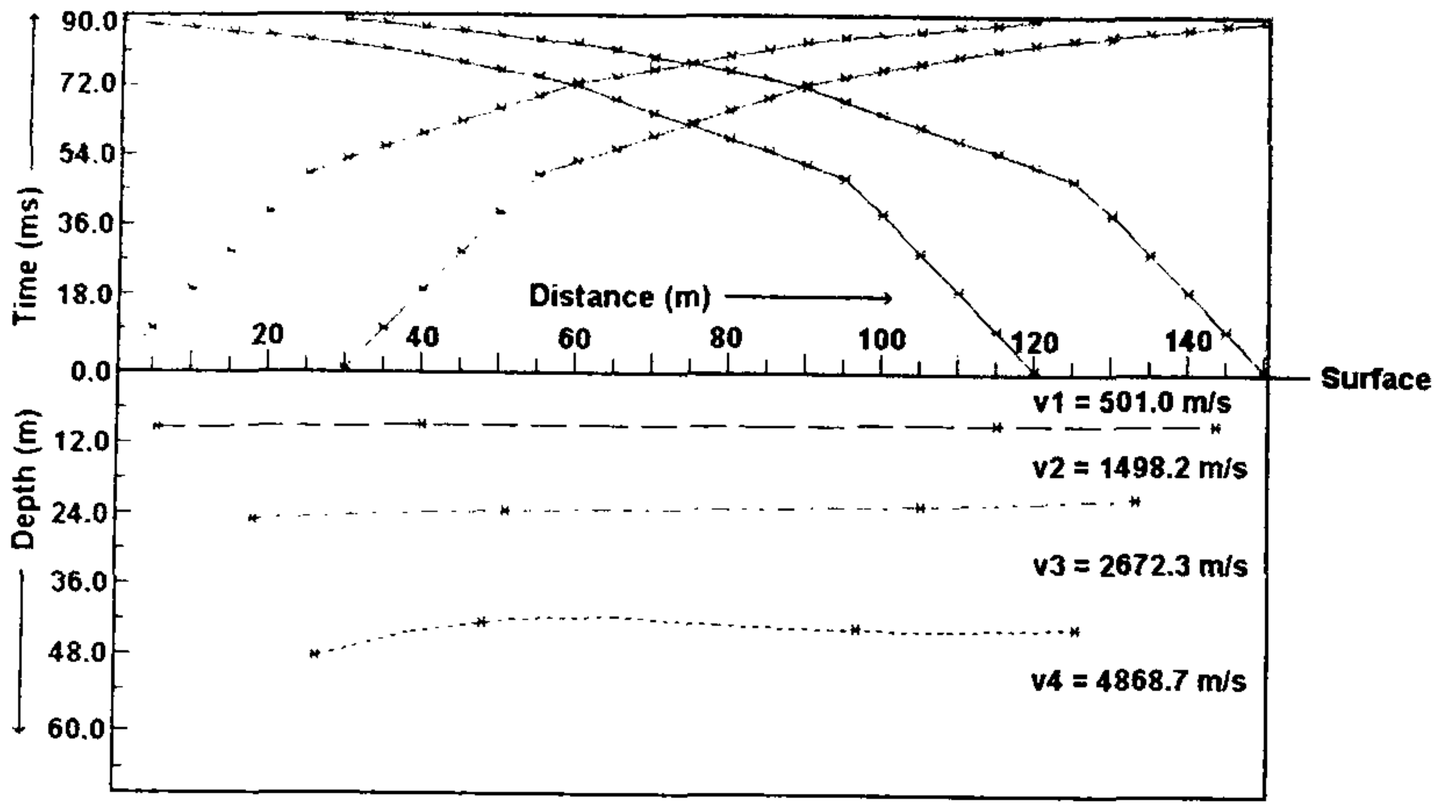

a

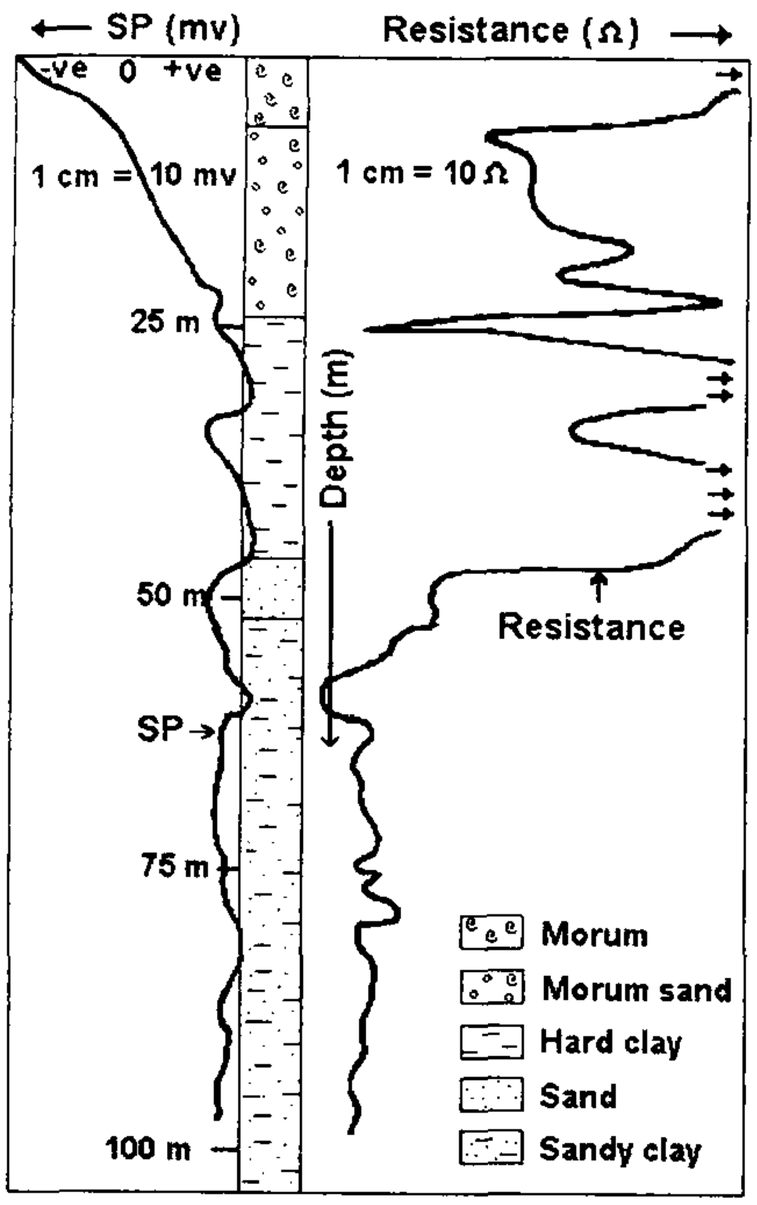

b

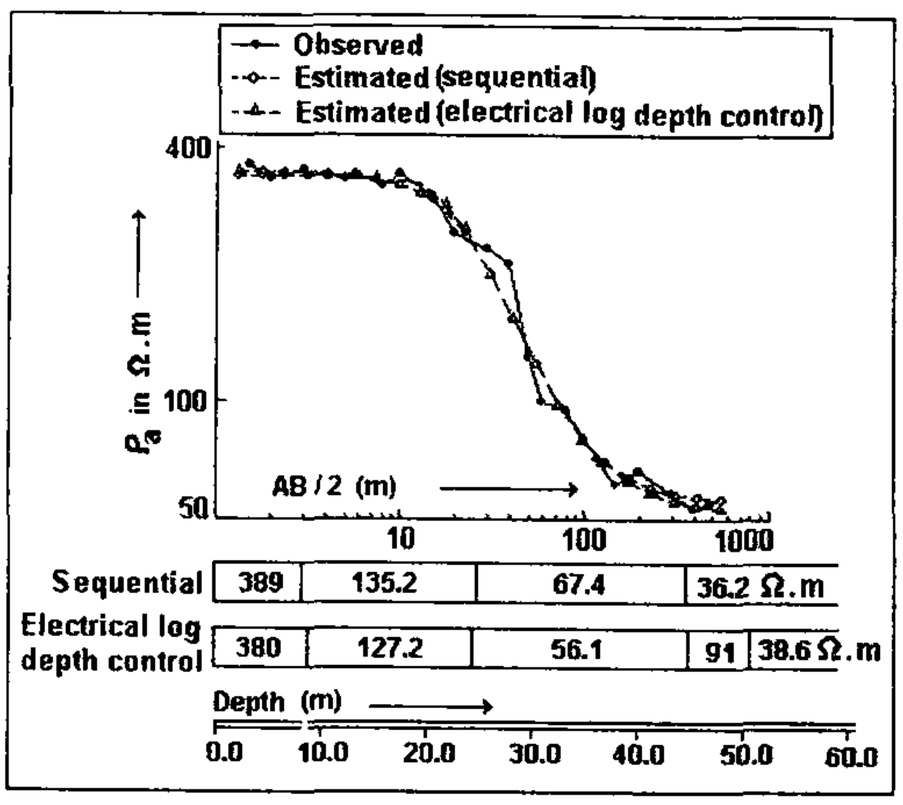

c

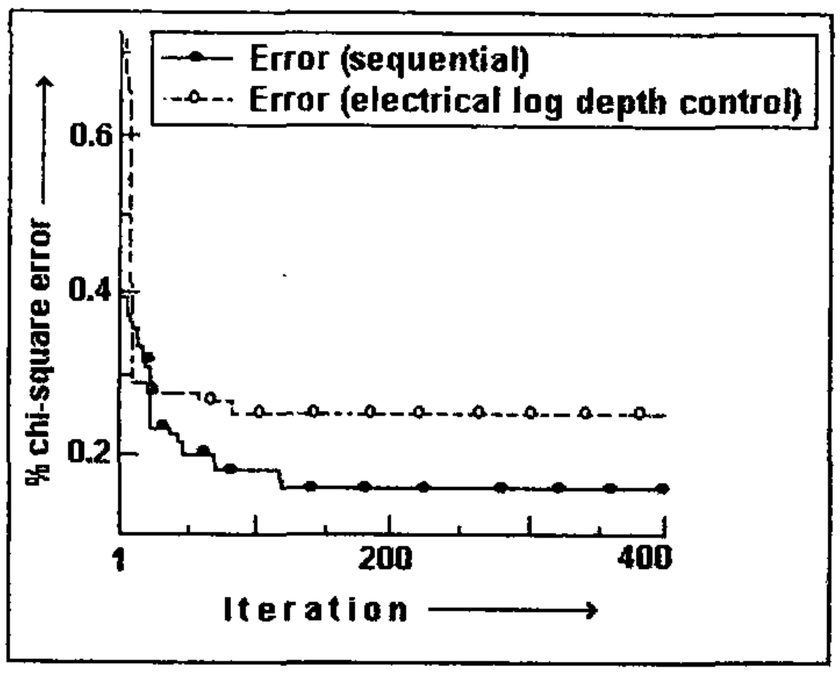

d

Figure 9 *a*, Time–distance curves and interpreted seismic section at Salboni; *b*, SP, point resistance and lithologs at Salboni; *c*, Observed and estimated VES curves by seismic and electrical log/litholog depth control at Salboni; *d*, Error curves for the joint application.

Table 4. Seismic and geoelectric parameters at Salboni

Estimate	v_1 (m/s)	v_2 (m/s)	v_3 (m/s)	v_4 (m/s)	v_5 (m/s)	ρ_1 (Ω.m)	ρ_2 (Ω.m)	ρ_3 (Ω.m)	ρ_4 (Ω.m)	ρ_5 (Ω.m)	h_1 (m)	h_2 (m)	h_3 (m)	h_4 (m)	h_5 (m)
Seismic (RINSE)	500	1498	2672	4868	–	–	–	–	–	–	9.0	15.3	21.8	∞	–
Geoelectric model (sequential)	–	–	–	–	–	389	135	67	36	–	8.8	15.5	21.5	∞	–
Geoelectric model (electrical log depth control)	–	–	–	–	–	380	127	56	91	39	9.1	15.2	22.0	6.1	∞

able from a nearby borehole (see Figure 5 *d*). A five-layer earth model is depicted from both the electrical and lithologs suggesting the existence of a probable aquifer at 46 m depth level which went undetected in seismic interpretation. Using the seismic and electrolog/litholog depth controls, the VES data are sequentially inverted to generate the layer parameters as tabulated in Table 4. The observed and estimated VES curves are shown in Figure 9 *c* with the error curves in Figure 9 *d*. It is evident that without this additional information the deeper aquifer could not have been delineated from seismic guided VES data inversion.

Conclusion

We have introduced a joint application scheme for the multi-sequential inversion of seismic refraction and vertical electrical sounding data. Both the synthetic and real field examples presented here undoubtedly establish the potentiality and accuracy of the scheme in delineating shallow aquifers even in a complex geological set-up. The algorithm as such does not have any depth restriction. The limitation is posed by the less penetrative power of the mechanical seismic sources to drive the signal deeper, thereby restricting the refraction data to shallower depths. This program is capable of generating seismo-electric subsurface models efficiently in 2D environment even on a laptop computer at-site cost-effectively. The practising hydrogeologists and engineers may use this software effectively in solving intricate geological problems related to groundwater exploration.

1. Sandberg, S. K., *Geophys. Prospect.*, 1993, **41**, 207–227.
2. Vozoff, K. and Jupp, D. L. B., *Geophys. J. R. Astron. Soc.*, 1975, **42**, 977–991.
3. Hering, A., Misiek, R., Gyulai, A., Ormos, T., Dobroka, M. and Dresen, L., *Geophys. Prospect.*, 1995, **43**, 135–156.
4. Breitzke, M., Dresen, L., Csokas, J., Gyulai, A. and Ormos, T., *Geophys. Prospect.*, 1987, **35**, 832–863.
5. Misiek, R., Liebig, A., Gyulai, A., Ormos, T., Dobroka, M. and Dresen, L., *Geophys. Prospect.*, 1997, **45**, 65–85.
6. Raiche, A. P., Jupp, D. L. B., Rutter, H. and Vozoff, K., *Geophysics*, 1985, **50**, 1618–1627.
7. Lines, L., Schultz, A. K. and Treitei, S., 57th SEG meeting, New Orleans, USA, 1987, pp. 814–816.
8. Dobroka, M., Gyulai, A., Ormos, T., Csokas, J. and Dresen, L., *Geophys. Prospect.*, 1991, **39**, 643–665.
9. Verma, S. K. and Venkataramana, D., *Boll. Geofis. Teor. Appl.*, 1995, **XXXVII**, 103–113.
10. Koefoed, O., in *Resistivity Sounding Measurements: Geosounding Principles I*, Elsevier, Amsterdam, 1979.
11. Beard, L. P. and Morgan, F. D., *Geophysics*, 1991, **5**, 874–883.
12. Jones, G. M. and Jovanovich, D. B., *Geophysics*, 1985, **50**, 1701–1720.
13. Nath, S. K., John, R., Singh, S. K., Sengupta, S. and Patra, H. P., *Comput. Geosci.*, 1996, **22**, 305–332.
14. Goldberg, D. E., in *Genetic Algorithms in Search Optimization*, Addison-Wesley Publishing Company, USA, 1989.
15. Sen, M. K. and Stoffa, P. L., in *Global Optimization Methods in Geophysical Inversion*, Elsevier, Amsterdam, 1995.
16. Chundru, R. K., Sen, M. K., Stoffa, P. L. and Nagendra, R., *Geophys. Prospect.*, 1995, **43**, 979–1004.
17. Fogel, D. B., in *System Identification Through Simulated Evolution: A Machine Learning Approach to Modelling*, Ginn Press, MA, 1991.
18. Shahid, S., Nath, S. K., Sircar, A. and Patra, H. P., *Acta Geophys. Pol.*, 1999, **XLVII** (in press).
19. Ghosh, D. P., *Geophys. Prospect.*, 1971, **19**, 769–775.

ACKNOWLEDGEMENTS. The authors are grateful to Dr M. Dobroka, University of Miskole, Hungary, Dr S. K. Sandberg, Rutgers University, USA, Dr H. P. Patra, IIT Kharagpur and the anonymous reviewers for critically reviewing the manuscript. A part of this work was supported by CSIR, Govt. of India, vide the sanction number (24/(0227))/95/EMR-II dated 19.12.1994

Received 21 July 1999; revised accepted 13 October 1999